



Bioactive engineered scaffolds based on PCL-PEG-PCL and tumor cell-derived exosomes to minimize the foreign body reaction

Zehong Xiang^{a,b}, Xinghua Guan^{a,b}, Zhifang Ma^a, Qiang Shi^{a,b,c,*}, Mikhail Pantelev^{d,e}, Fazly I. Ataullakhanov^{d,e}

^a State Key Laboratory of Polymer Physics and Chemistry, Changchun Institute of Applied Chemistry, Chinese Academy of Sciences, Changchun, Jilin 130022, China

^b University of Science and Technology of China, Hefei, Anhui 230026, China

^c Key Laboratory of Polymeric Materials Design and Synthesis for Biomedical Function, Soochow University, Suzhou 215123, China

^d Dmitry Rogachev Natl Res Ctr Pediat Hematol Oncol, 1 Samory Mashela St, Moscow, 117198, Russia

^e Faculty of Physics, Lomonosov Moscow State University, Leninskie Gory, 1, build. 2, GSP-1, Moscow 119991, Russia



ARTICLE INFO

Keywords:

Exosomes
Macrophages
Inflammation
Polarization
Engineered scaffolds

ABSTRACT

Long-term presence of M1 macrophages causes serious foreign body reaction (FBR), which is the main reason for the failure of biological scaffold integration. Inducing M2 polarization of macrophages near scaffolds to reduce foreign body response has been widely researched. In this work, inspired by the special capability of tumor exosomes in macrophages M2 polarization, we integrate tumor-derived exosomes into biological scaffolds to minimize the FBR. In brief, breast cancer cell-derived exosomes are loaded into polycaprolactone-b-polyethylene glycol-b-polycaprolactone (PCL-PEG-PCL) fiber scaffold through physical adsorption and entrapment to construct bioactive engineered scaffold. In cellular experiments, we demonstrate bioactive engineered scaffold based on PCL-PEG-PCL and exosomes can promote the transformation of macrophages from M1 to M2 through the PI3K/Akt signaling pathway. In addition, the exosomes release gradually from scaffolds and act on the macrophages around the scaffolds to reduce FBR in a subcutaneous implant mouse model. Compared with PCL-PEG-PCL scaffolds without exosomes, bioactive engineered scaffolds reduce significantly inflammation and fibrosis of tissues around the scaffolds. Therefore, cancer cell-derived exosomes show the potential for constructing engineered scaffolds in inhibiting the excessive inflammation and facilitating tissue formation.

1. Introduction

Recently, tissue engineering has been developed as a major tool of repairing and remodeling damaged tissues and organs [1–4]. Tissue engineering scaffolds with guide tissue regeneration and control the tissue structure in damaged parts have played a vital role in tissue engineering. Foreign body reaction (FBR) caused by tissue engineering scaffolds leads to prolonged or frustrated repair or fibrosis that further results in the loss of functions partly or completely, which is a major limitation of tissue engineering scaffolds [5,6]. The key role played by host macrophages against biomaterials has been increasingly recognized. Macrophages are highly plastic and can differentiate along a phenotypic axis between two poles of ‘M1’ (inflammatory) and ‘M2’ (anti-inflammatory) and active in the process of fibrous tissue formation and wound healing [6–8]. Increasing evidences show that the balance of macrophage classical (M1) and altered (M2) activation governs the fate of tissue regeneration [6,9–12]. Although the initial presence of M1 macrophages facilitates a neces-

sary inflammatory response, a prolonged M1 dwell causes a severe FBR, resulting in chronic inflammation and failure of biomaterials integration. Therefore, minimizing unnecessary inflammation and promoting macrophage M2 polarization around the biomaterial is the promising strategies for successful implanted biomaterials and devices [13,14].

The regulation of exosomes in immune response has been widely documented. Exosomes are 40–150 nm extracellular vesicles released by all cell types. Similar to cells, exosomes contain proteins, RNA, and DNA with a lipid bilayer [15–17]. The immunological activities of exosomes in tumors are complex and dynamics. Cancer cell-derived exosomes act as a source of tumor antigens which are presented to the activated T-cells and directly activate NK cells [18–20]. Specially, cancer cell-derived exosomes are capable of promoting M2 polarization of macrophage in tumor immunity [21,22]. Therefore, it is expected that cancer cell-derived exosomes can be harnessed to construct bioactive engineered scaffolds to minimize the unnecessary immune reactions. However, the safety and availability of cancer cell-derived exosomes on tissue engineering are scarcely investigated.

* Corresponding author at: State Key Laboratory of Polymer Physics and Chemistry, Changchun Institute of Applied Chemistry, Chinese Academy of Sciences, Changchun, Jilin 130022, China.

E-mail address: shiqiang@ciac.ac.cn (Q. Shi).

<https://doi.org/10.1016/j.bbiosy.2022.100055>

Received 23 January 2022; Received in revised form 31 May 2022; Accepted 8 June 2022

2666-5344/© 2022 The Authors. Published by Elsevier Ltd. This is an open access article under the CC BY-NC-ND license

(<http://creativecommons.org/licenses/by-nc-nd/4.0/>)

In the tissue engineering scaffold, micro/nano fiber scaffolds of biodegradable polymers, such as polycaprolactone, provided initial mechanical support and a 3D niche allowed the tissue to regenerate are becoming more and more popular among researchers [23]. However, the hydrophobicity of polycaprolactone leads to a large amount of protein adsorption and inhibits loading of hydrophilic materials, which limits its application in biomedicine. We have previously developed a fiber scaffold with polycaprolactone-b-polyethylene glycol-b-polycaprolactone [24]. The introduction of polyethylene glycol block in the polymer backbone can speed up the loading of hydrophilic materials and prevent the adsorption of proteins and platelets [25]. Therefore, generation of bioactive engineered scaffolds based on PCL-PEG-PCL scaffolds with the facile way is highly desired.

In this work, inspired by the special capability of tumor exosomes in macrophages M2 polarization, we design the bioactive engineered scaffolds by loading 4T1 cell-derived exosomes on PCL-PEG-PCL scaffold to minimize unnecessary inflammation and fibrosis caused by FBR. Mouse breast cancer cells are chosen as donor of exosomes, and the biological safety of exosomes is evaluated firstly *in vivo*, because some tumor exosomes are reported to induce cell cancerous, promote cancer cell growth and metastasis [26–28]. We demonstrate tumor exosomes exhibit no carcinogenicity for normal mouse within 6 months. Then, PCL-PEG-PCL scaffolds are prepared by electrospinning technique. Due to high water adsorption and 3D structure of the scaffolds, exosomes are easily loaded onto the scaffolds to construct bioactive engineered scaffold. Finally, the scaffolds are implanted in the mouse to investigate the immune manipulation of biomaterials. The exosomes are gradually released and act on the macrophages near the scaffolds to induce macrophages M2 phenotype. Therefore, cancer cell-derived exosomes show the potential for tissue engineered scaffolds construction of implanted biomaterials in inhibiting the excessive inflammation and facilitating tissue formation.

2. Materials and methods

2.1. Materials

Stannous octoate, ϵ -caprolactone and PEG-10⁴ were purchased in Energy Chemical, antibody of CD68(Alexa Fluor @647, eBioY1/82A), CD86(PE, IT2.2), CD206(FITC, C068C2) were purchased from thermoFisher Scientific. All cells were purchased from Beyotime Biotechnology of Shanghai. Dimethylformamide (DMF), trimethylamine, ethylenediamine, acrylamide, dichloromethane (DCM), tetrahydrofuran (THF), acetone, and xylene were reagent-grade products. Other reagents were AR-grade and used without further purification. Phosphate-buffered saline (PBS 0.9% NaCl, 0.01 M phosphate buffer, PH 7.4) was prepared freshly.

2.2. Extraction of breast cancer cell-derived exosomes

The growth and metastasis characteristics of 4T1 cells in mice are very similar to human breast cancer [29]. So breast cancer cell is chosen as exosomal donor. 4T1 cells are seeded into petri dish. After incubation with 5% CO₂ at 37°C until cell confluency reach 80%–90%, the cultural medium is renewed by RPMI 1640 supplemented 10% FBS and 100 μ M CoCl₂ [30]. The culturing is followed for another 48 h, and conditioned culture medium is collected. The 4T1-derived exosomes (Exos, the latter exosomes mean the same thing) are isolated by density-gradient centrifugation as described previously [31]. Specifically, conditioned culture medium is by centrifugation at 300rpm for 15min to isolate free cells. And the supernatant is by centrifugation at 1000rpm for 30min to isolate free cellular debris. The exosomes are isolated by Exosome Purification Kit (CELL guidance systems) from the last supernatant. The isolated exosomes are preserved in liquid nitrogen. Set the concentration to 10 μ g/ml with each use. The size of exosomes is evaluated by dynamic light scattering and transmission electron microscopy.

2.3. Safety of breast cancer cell-derived exosomes

All animal procedures are performed in accordance with the Guidelines for Care and Use of Laboratory Animals of Changchun Institute of Applied Chemistry (Chinese Academy of Sciences) and approved by the Animal Ethics Committee of Changchun Institute of Applied Chemistry (Chinese Academy of Sciences). For each experimental group, 6 female KM mice with 6 weeks of age (about 30g) are used and all mice were randomly selected. The cells and living bodies in this study were derived from mice.

In order to verify the safety of Exos, whose tumorigenicity and promote cancerous have been researched. In particular, mice are injected with Exos(100 μ L) by tail intravenous injection and are raised for 6 months after that. Accurate diagnosis of cancer slices is the fundamental process for improving treatment response and prognosis. H&E has been widely used for staining pathological slices in most countries [32]. Through tissue analysis of these mice, tumorigenicity can be assessed.

On the other hand, the mouse metastasis model is designed to demonstrate the tumor-promoting properties of Exos [33]. In brief, 4T1 cells (1×10^6 per mouse) are injected into tail vein of KM mouse to generate the lung metastatic 4T1 mammary adenocarcinoma model. Above this, the experimental group is injected with Exos and the mice with 4T1 cells but no Exos are control. All mice are euthanized and sacrificed after feeding for 2 weeks. Histological analysis observed metastatic tumors in the lungs of mice, and the number of tumors is used to assess the severity of the cancer. In addition, the lung metastatic U14 cervical adenocarcinoma model is established to assess the tumor-promoting effect of Exos.

2.4. Exosomes induce macrophage into M2 polarization

The RAW264.7 cells are stimulated with LPS (100ng/mL) for 6 h. Then, the LPS-stimulated macrophages are incubated with exosomes for 24 h [34]. The supernatant in each group is collected and measured the concentrations of TNF- α and IL-10 in samples by mouse TNF- α and IL-10 Enzyme-Linked Immuno Sorbent Assay KIT. And immunofluorescent staining of CD206, CD86 and DAPI is performed on macrophages to mark the M2 macrophages, M1 macrophages and cell nucleus [35,36]. M2 polarization of macrophages is detected by laser confocal method. The polarization of the cells is also characterized by flow cytometry.

2.5. Anti-inflammation assessment in vivo

Acute peritonitis model is designed according to the report by Wu et al. [37]. In brief, mice are firstly intraperitoneally injected with sterile zymosan solution (0.5 mL, 2 mg/mL). After 12 h, Exos are injected into the mice enterocoelia, and PBS-injected mice are used as the control group. All mice are euthanized and sacrificed after feeding for 24h. 2 ml PBS is used to lavage belly, the cell in lavage liquid is centrifuge with 1500rpm for 5min. The immune cells are marked by CD68 and observed by laser scanning confocal microscope. The concentrations of IL-6, TNF- α and IL-10 in supernate are measured using mouse Enzyme-Linked Immuno Sorbent Assay KIT.

2.6. Preparation and characterization of bioactive engineered scaffolds

PCL-PEG-PCL scaffolds are prepared by electrostatic spinning in a previous job [24]. Dried PEG-10⁴ (2 g) is dissolved in 25 ml of dried methylbenzene in an ampoule. Then, dried ϵ -caprolactone (18 g) and 60 mg of stannous octoate are added (–OH: catalyst = 3: 1). The solution is degassed with freeze–pump–thaw cycles and the reaction is performed at 115°C for 48 h. After the reaction is completed, the PCL-PEG-PCL triblock copolymer is obtained after precipitation with ether. And PCL-PEG-PCL scaffolds are prepared with PCL-PEG-PCL solution (20 wt% in DMF) by electrospinning technique. The microstructure and mechanical properties of the scaffold are characterized by universal testing machine

(mechanical tester Instron 1211 instrument) and scanning electron microscope (SEM, Sirion-100, FEI, USA).

The conditioned culture medium of 4T1 cells is incubated with CM-Dil (Cell Plasma Membrane Staining (1,1'-dioctadecyl-3,3,3',3'-tetramethylindocarbocyanine perchlorate, a red dye), 4 $\mu\text{g}/\text{mL}$ in RPMI 1640) at 37°C for 30 min. The Dil labeled exosomes are isolated from cell culture supernatant by Exosome Purification Kit as previously described and used to fabricate PCL-PEG-PCL/Dil-labeled Exos. In brief, 200 μL Dil-labeled Exos solution is assimilated in $1 \times 1 \text{ cm}^2$ PCL-PEG-PCL film because of the high water absorption of the film. The fiber is then lyophilized within 1 h to obtain bioactive engineered scaffold (PCL-PEG-PCL@Exos). Then, bioactive engineered scaffold is immersed in 1ml PBS for 24 h, then the leaching solution is collected, and the patch is refreshed with 1ml PBS each day. Leaching solution for each of the 6 days is collected, the release of exosomes is determined through exciting at 549nm with a microplate reader and observe the fluorescence intensity at 565nm. The exosome release curve of the load on the PCL-PEG-PCL casting scaffold was measured by the same method.

2.7. Hemolysis and BCI assay

The fresh blood is collected in an EDTA-containing anticoagulation tube. Then the red blood cells are isolated from the blood by centrifugation at 1000 rpm for 10 min and subsequently rinsed by PBS three times. Bioactive engineered scaffold containing Exos of varying mass (0 μg , 0.5 μg , 1 μg , 1.5 μg , 2 μg) are incubated with red blood cells for 2 h at 37°C. The red blood cells (RBCs) in PBS and water are set as negative and positive control, respectively. The RBCs are removed by centrifugation (3000 rpm, 5 min), and the supernatant is transferred to 96-well plates and its absorbance at 541 nm is measured using a microplate reader. The hemolysis ratio (HR) was calculated according to the following formula:

$$\text{Hemolysisrate (\%)} = \frac{OD_{\text{sample}} - OD_{\text{neg}}}{OD_{\text{pos}} - OD_{\text{neg}}} \times 100\% \quad (1)$$

Whole blood (200 μL) is dropped on different scaffolds, and then 20 μL of 0.2 M CaCl_2 solution is added to the blood. The control group was produced by dropping blood on glass. Each sample is incubated for 5 min at 37°C. Next, distilled water (25 ml) is carefully added to the beaker and incubated at 37°C with shaking at 30 rpm for 10 min. Finally, the blood-clotting index (BCI) of nanofibers was calculated from the following equation:

$$\text{BCI} = \frac{OD_{\text{sample}}}{OD_{\text{blank}}} \times 100\% \quad (2)$$

where OD_{sample} is the absorbance of the test samples, and OD_{blank} is the absorbance of the contrast group.

2.8. Bioactive engineered scaffolds induce macrophage into M2 polarization

The RAW264.7 cells are stimulated with LPS (100ng/mL) for 6 h. Then, the LPS-stimulated macrophages are incubated with PCL-PEG-PCL@Exos scaffolds for 24 h. The supernatant in each group is collected and centrifuged and measured the concentrations of IL-6 and IL-10 in samples by mouse IL-6 and IL-10 Enzyme-Linked Immuno Sorbent Assay KIT. And immunofluorescent staining of CD206 and DAPI is performed on macrophages. M2 polarization of macrophages is detected by laser confocal method.

2.9. Bioactive engineered scaffolds inhibit inflammation in vivo

The air-pouch model of inflammation is used according to the method of Vasconcelos et al. [38]. Briefly, KM mice (about 25g) are injected subcutaneously in the dorsal area with 5 mL of sterile air that caused the formation of an air pouch. A reinforcement of the air pouch is performed 5 days latter through a second subcutaneous injection of

3 mL of sterile air. Scaffolds are implanted 24 h after the second subcutaneous injection then LPS (100ng/ml, 100 μL) is injected into the air-pouch. Mice are anaesthetized as described above and the skin covering the air pouch area is shaved and cleaned. A surgical incision is made, the PCL-PEG-PCL@Exos and PCL-PEG-PCL@PBS (PCL-PEG-PCL scaffold with PBS) scaffolds are placed inside the air pouch and the incision is sutured. The mice with air-pouch but no scaffold and LPS are control. For each experimental group, 6 male KM mice with 6 weeks of age are used. All mice are euthanized and sacrificed after feeding for 3 days. 2 ml PBS is used to lavage the air-pouch, lavage liquid is processed and analyzed the same as before.

2.10. Bioactive engineered scaffolds inhibit foreign body reaction in vivo

The effect of bioactive engineered scaffold to foreign body response is verified by implantation of scaffold into mouse skin. In brief, the scaffolds are implanted into the mice skin, the sham operation group is set as control. All mice are euthanized after 30 days at room temperature, the tissues around the scaffolds are removed and analyzed. These tissues are treated with H&E staining and Masson staining respectively. Besides, these tissues are treated with trypsin to produce scattered cells. The digested cells are further labeled with CD206 and CD86 antibodies, and all cells are labeled with DAPI. The cells are observed by confocal laser, and the fluorescence intensity and positive cells number in each field are calculated by image J software.

2.11. Exosomes promote macrophage M2 polarization via Akt/ PI3K

The mechanism of the exosomes (4T1 cells exosomes) promoting the polarization of macrophages is researched [39]. In brief, the RAW264.7 cells are stimulated with LPS (100ng/mL) for 6 h. Then, the LPS-stimulated macrophages are incubated with exosomes for 24 h. The role of exosomes in macrophage polarization is investigated in the presence and absence of 100 $\mu\text{g}/\text{ml}$ LY294002 (Abcam), Akt/ PI3K signaling pathways inhibitor. The supernatant in each group is collected and centrifuged. The concentrations of TNF- α , IL-6 and IL-10 in samples are measured using a mouse TNF- α and IL-10 Enzyme-Linked Immuno Sorbent Assay KIT. And immunofluorescent staining of CD206 and DAPI is performed on macrophages. M2 polarization of macrophages is detected by laser confocal method.

2.12. Statistical analysis

The BCI, hemolysis ratio, and IL-10, TNF- α level and other data are given as means \pm SD. Statistical analysis is performed using Origin Software and Image J, with post hoc analysis by Bonferroni's multiple comparison tests when appropriate. A non-parametric test (Mann-Whitney test) was used to determine differences between the treatment groups, as indicated in the figure legends. Differences are considered statistically significant at $P \leq 0.05$.

3. Results

3.1. Extraction and separation of breast cancer cell-derived exosomes

Here, 4T1 cells are chosen as donor of exosomes. Prior to the study on exosome-guided cell conversion, cobalt chloride is added to induce 4T1 cells to produce the required exosomes. The exosomes are obtained with Exosome Purification Kit (Fig. 1A). After isolation of exosomes from the supernatant of hypoxia induced 4T1 cells, the purified exosomes are characterized in morphology, size, and surface marker expression. The dynamic light scattering (DLS, Fig. 1B) and transmission electron microscopy (TEM, Fig. 1C) observation reveal that the 4T1- derived exosomes seem like round vesicles with a mean diameter of about 50nm (Fig. 1C). Further, western blot analyses are performed to examine the presence of confirmed exosomal proteins, including CD63 and TSP70

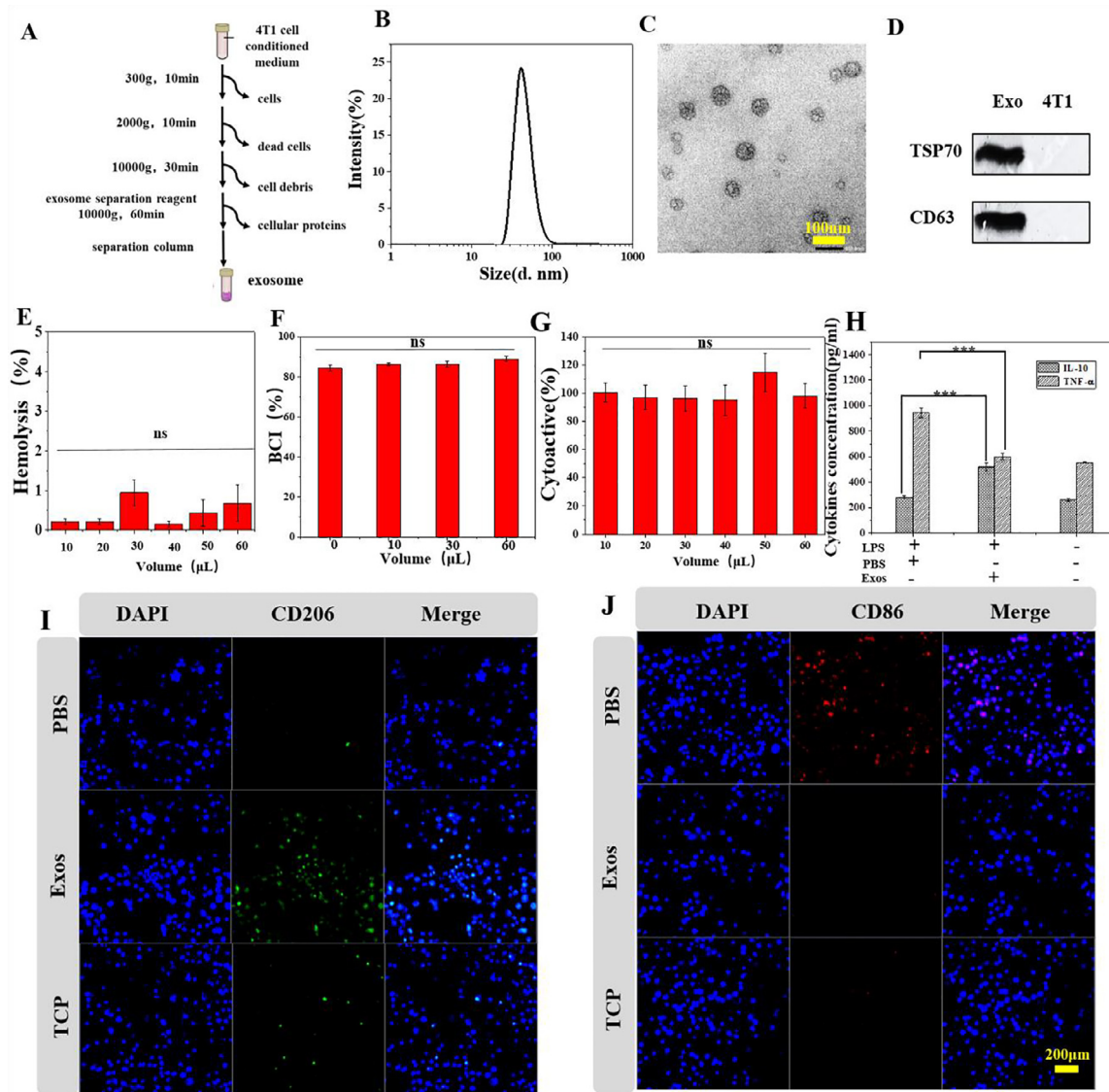


Fig. 1. Isolation and characterization of exosomes. (A) Isolation flowchart of 4T1 cell exosomes. (B) Dynamic light scattering of exosomes. (C) The TEM image of exosomes. (D) Western blot analysis of CD63 and TSP70 in 4T1 cells-derived exosomes and 4T1 cells. Hemolysis (E), BCI (F) and cytotoxicity (G) of exosome solution with different volumes. (H) the concentration of TNF- α and IL-10 in cell supernatant of different groups. (I) and (J) Confocal laser images of macrophages after different treatments. TCP is normal macrophage without special treatment. PBS is the LPS-stimulated macrophages that were incubated with PBS for 24 h. Exo is the LPS-stimulated macrophages that were incubated with exosomes for 24 h, green fluorescence represents CD206, green fluorescence represents CD86. The data are shown as the means \pm S.D. from three independent experiments (with three replicates each); ***p < 0.001 indicates significant differences between the indicated columns.

(Fig. 1D). These results support that 4T1-derived exosomes are successfully prepared with typical morphological and molecular features of exosomes.

3.2. Breast cancer cell-derived exosomes promote macrophages into M2 polarization

First, the biocompatibility of exosomes at the cellular level was studied. A hemolysis rate of less than 5% and a low coagulation index indicate that 4T1 exosomes do not cause hemolysis and coagulation (Fig. 1E, F). And cytotoxicity data further shows that exosomes do not affect cell survival (Fig. 1G). Then, exosomes are injected into cancer mice and normal mice to study the safety of exosomes *in vivo*. Mouse metastasis tumor model is established to evaluate the safety of 4T1 exosomes *in vivo*. The safety of exosomes is evaluated with the number of pulmonary nodules. The more lung nodules, the greater the ability of exosomes to

promote tumor cell metastasis. Fig. S1A and B represent the images and H&E staining images of the mice lung in different groups. The quantification of the nodules number confirms that the exosomes have no effect on the development of 4T1 tumors and U14 tumors (Fig. S1C). Meanwhile, the H&E staining of other organs of each group (Fig. S2) show no lesions. The results of H&E staining images of organs from normal mouse and mouse injected with exosomes for 6 months demonstrate that exosomes do not cause carcinogenicity (Fig. S1D, E).

One of the reasons for the immune evasion of tumor cells is to make the macrophages around the tumor undergo M2 polarization. So the effect of exosomes on macrophages is further researched. LPS-stimulated macrophages are treated with exosomes, the cytokine TNF- α (Marker factor secreted by M1 macrophages) concentration in the cell supernatant of the exosomes group is significantly lower than that of the PBS group and the IL-10 (Marker factor secreted by M2 macrophages) concentration in the cell supernatant is opposite (Fig. 1H). The confocal

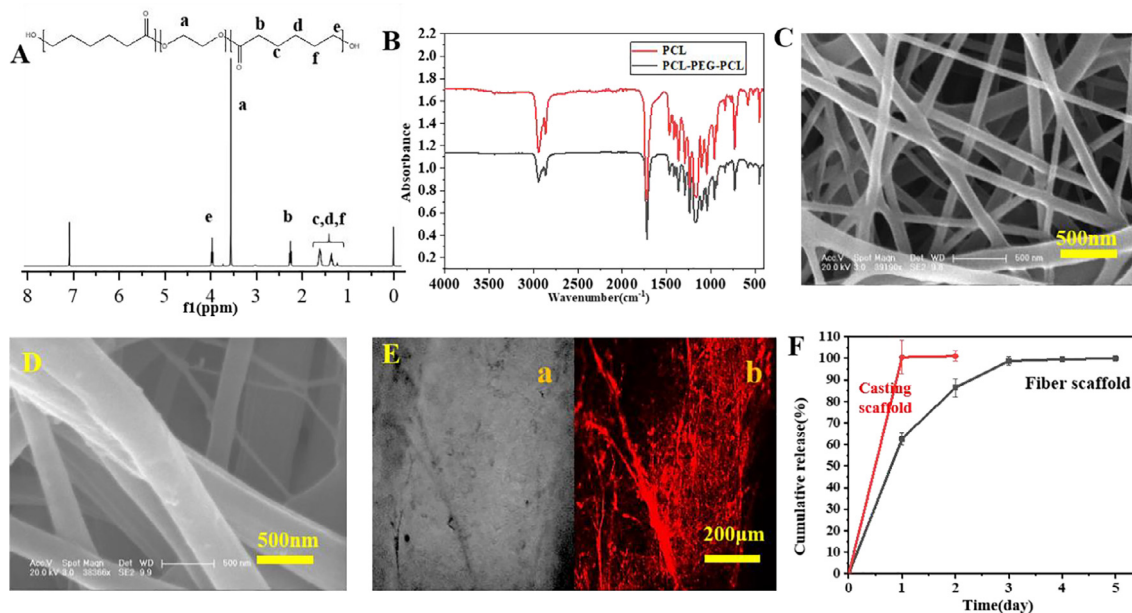


Fig. 2. The characterization of bioactive engineered scaffold. (A) ^1H NMR spectrum of PCL-PEG-PCL in CDCl_3 and (B) FTIR spectra of PCL and PCL-PEG-PCL. The SEM image of PCL-PEG-PCL scaffold (C) and PCL-PEG-PCL@Exos scaffold (D). (E) Confocal laser image of the scaffolds loaded with exosomes, (a) Bright field (b) 549nm. (F) Cumulative release curve of exosomes on the casting scaffolds and fiber scaffold.

laser images indicate that the $\text{CD}206^+$ cells in Exo group increase compared with that in PBS group, and the $\text{CD}86^+$ cell decrease obviously (Fig. 1 I and J). From the flow cytometry (Fig. S3), M1 macrophages count decreased from 10% to 1.46%, and M2 macrophages count increased from 1.83% to 9.74% after treated by exosomes. The result proves that exosomes can promote the macrophages (RAW 264.7) in inflammatory conditions to M2 polarization. At the same time, peritonitis experiment in mice further confirms that exosomes can inhibit inflammation *in vivo* (Fig. S4).

3.3. Bioactive engineered scaffolds induce macrophage into M2 polarization

Through ring-opening polymerization, a PCL-PEG-PCL triblock polymer is successfully synthesized in this study (Fig. 2A, B). The PCL-PEG-PCL scaffold is prepared by electrostatic spinning, and the SEM image of the scaffold show the diameter of the fibers are about 100nm (Fig. 2C). The elongation is about 58%, and the yield strength is about 4MPa (Fig. S5). Then, exosomes are loaded onto the PCL-PEG-PCL scaffold to construct bioactive engineered scaffold by drop exosome solution onto the scaffold. Due to the loading method, the adsorption efficiency of exosome was expected to be nearly 100%. The exosomes are marked with CM-Dil, and the PCL-PEG-PCL@Exos scaffold is observed by laser scanning confocal microscope. The particles on the fiber (Fig. 2D) confirm and the red fluorescence on the fiber surface (Fig. 2E) that the exosomes are successfully loaded onto the scaffold with slight swelling of scaffold fibers. The release of exosomes on fiber scaffold and casting scaffold was compared, the release of exosomes can last for three days in fiber scaffold but only one day in casting scaffold (Fig. 2F). That is because the larger the specific surface area, the slower the release. Indicating that the exosomes have enough time to induce the macrophages near the fiber scaffolds to M2 polarization.

In order to verify the ability of PCL-PEG-PCL@Exos scaffolds in M2 polarization, different scaffolds are used to incubate the LPS-stimulated macrophages. The fluorescence images (Fig. 3A) and quantitative data (Fig. 3B) of M2 macrophages exhibit most M2 polarized macrophages appear after treated by PCL-PEG-PCL@Exos. On the contrary, the number of M1 macrophages decreased significantly (Fig. 3Aa'–f' and C).

And the more exosome load, the better polarization effect. The anti-inflammatory factors (IL-10) in the PCL-PEG-PCL@2Exos and PCL-PEG-PCL@1.5Exos group are higher than those in the LPS group (Fig. 4D), while the pro-inflammatory factors (IL-6) are significantly lower than those in the LPS group (Fig. 4E). Combine all the results, the scaffolds with $2\mu\text{g}$ exosomes (PCL-PEG-PCL@2Exos) have the best capability to induce macrophage into M2 polarization. Besides, the blood compatibility of scaffolds is also evaluated, the hemolysis rate, BCI, PT and APTT of scaffolds are measured. The results show all the scaffolds with exosomes do not cause hemolysis and coagulation (Fig. S6A–C).

3.4. Bioactive engineered scaffolds inhibit foreign body reaction in vivo

To evaluate the foreign body response during long-term implantation, different scaffolds are implanted under the skin of Kunming mouse for one month. The operation procedure is shown in Fig. 4A. Before the implantation, the degradation of PCL-PEG-PCL scaffolds in PBS (37°C) and corresponding change of PH in solution are tested *in vitro*. The weight of the scaffolds is monitored at regular intervals to detect the degradation under physiological conditions. The SEM images of the fiber scaffolds before immersion and after 30-day immersion are shown in Fig. 4B and 4C, respectively. The fiber structure of the scaffold deforms significantly after 30-day immersion. And the weight of scaffold is only about 85% of original samples (Fig. 4D). Correspondingly, the PH of the soak solution changes from 7.5 to 7.25 after 30-day immersion (Fig. 4E).

Then, different scaffolds are implanted under the skin of mouse. The scaffolds and the tissue around are taken out after 30 days. Firstly, cells on the scaffold are labeled with CD206 antibody and DAPI, respectively. The confocal image of the PCL-PEG-PCL@2Exos (Fig. S7A) and PCL-PEG-PCL@PBS (Fig. S7B) show the distribution of $\text{CD}206^+$ cells on the surface of scaffolds. These images are processed using image J, and the intensity of green fluorescence (FITC, fluorescent dye of anti-CD206) (Fig. S7C) in different groups are compared. The PCL-PEG-PCL@2Exos scaffold has more $\text{CD}206^+$ cells than that with the PCL-PEG-PCL@PBS (PCL-PEG-PCL scaffold with PBS). After that, the tissue around the scaffold is cut up and the cells digested with trypsin for analysis. M2 macrophages are labeled with anti-CD206, M1 macrophages are labeled with anti-CD86, and then all cells are labeled with DAPI. As

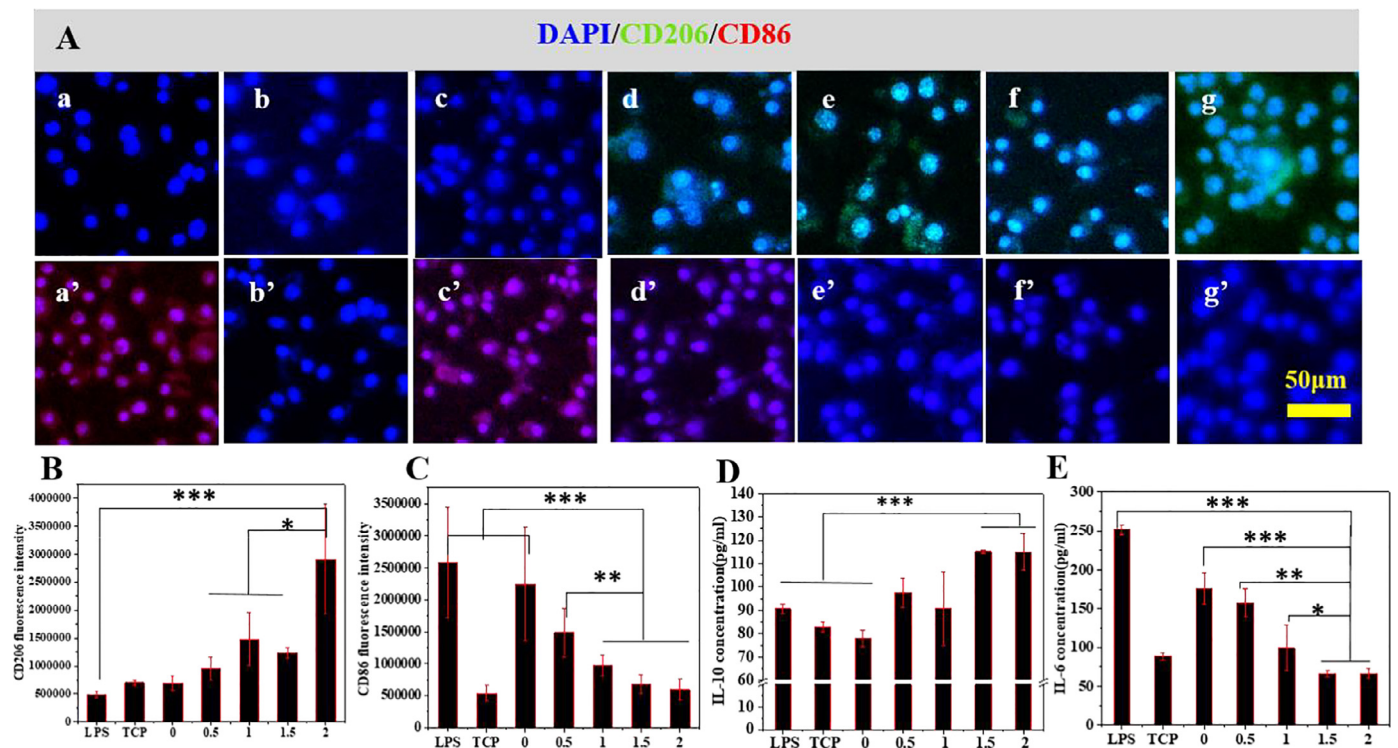


Fig. 3. Bioactive engineered scaffold induce macrophage into M2 polarization. (A) Confocal laser images of macrophages after different treatments, a and b are the negative control and positive control, respectively. c-g stands for the LPS-stimulated macrophages that are incubated with different scaffolds (0, 0.5, 1, 1.5, 2) for 24 h. Blue fluorescence represents DAPI, green fluorescence represents CD206, red fluorescence represents CD86. 0-2 are PCL-PEG-PCL scaffolds loaded with varied content of exosomes, respectively (PCL-PEG-PCL@xExos). And the number x denotes the amount of exosomes (μg) loaded on the PCL-PEG-PCL scaffolds. (B) and (C) CD206 and CD86 fluorescence intensity in confocal laser images of different groups. The concentration of IL-10 (D) and IL-6 (E) of different groups. The data are shown as the means \pm S.D. from three independent experiments (with three replicates each); * $p < 0.05$, ** $p < 0.01$, *** $p < 0.001$ indicates significant differences between the indicated columns.

shown in Fig. 4F and I, the tissue around the PCL-PEG-PCL@2Exos scaffold has more M2 macrophages, while the scaffold with PBS possesses more M1 macrophage. The quantification of the fluorescence intensity of CD206 (Fig. 4G) and CD86 (Fig. 4J) further supports this result. The proportion of CD206⁺ cells and CD 86⁺ cells in total cells are further compared, and the CD206⁺ cells account for about 15% of the total cells in exosomes-loaded scaffold group, which is far more than that of the PCL-PEG-PCL@PBS group (Fig. 4H). On the contrary, the CD86⁺ cells account for about 30% of the total cells in PCL-PEG-PCL@PBS scaffold group, which is much higher than that of the PCL-PEG-PCL@2Exos group (Fig. 4K).

Further, tissue analysis is carried out to evaluate the anti-inflammatory capability of exosomes. The tissues are stained with H&E and Masson, respectively. The H&E staining images (Fig. 4L a-c) show the tissues around PCL-PEG-PCL@PBS have more number of inflammatory cell aggregation compared with that of PCL-PEG-PCL@2Exos. The neutrophils in the tissues are counted (Fig. 4M), and the number of neutrophils in the PCL-PEG-PCL@2Exos group is similar to that of normal tissues, further confirming the high capability of the bioactive engineered scaffolds to in suppressing excessive inflammation. The multinucleated giant cells appear in PCL-PEG-PCL@PBS group (Fig. 4L-c) but not in PCL-PEG-PCL@2Exos (Fig. 4 L-b) group demonstrate that the bioactive engineered scaffolds can reduce foreign body reaction. Furthermore, masson staining is used to analyze the collagen fiber of the tissue near the scaffold (Fig. 4L d-f). As shown in Fig. 4L, the collagen fiber of the tissue near the PCL-PEG-PCL@PBS scaffold is dense. On the contrary, the density of collagen in the tissues around PCL-PEG-PCL@2Exo is similar to that in the normal subcutaneous tissue, with the normal migration and growth of cells. The quantitative data of collagen density (Fig. 4N) further demonstrate that, compared with the PCL-PEG-

PCL@PBS, the bioactive engineered scaffolds have higher ability to reduce foreign body reaction.

3.5. Exosomes promote macrophage M2 polarization via Akt/ PI3K

To reveal the role of exosomes in macrophage polarization, the pathway of exosomes in promoting macrophage M2 polarization is investigated tentatively. The typical inhibitor for Akt/ PI3K pathway, LY294002 is added to the media of macrophage and exosomes. As shown in Fig. 5A, the exosomes promote the macrophages into M2 polarization. And when the phosphatidylinositol 3-kinase (PI3K) are inhibited with LY294002, the fluorescence intensity (Fig. 5B) and proportion (Fig. 5C) of M2 macrophages are reduced substantially. compared with that of exosomes group, IL-10 level decreases obviously after PI3K inhibition (Fig. 5D). In the contrary, the concentration of IL-6, TNF- α (proinflammatory factor) are remarkably enhanced. Thus, the PI3K/Akt signal pathway may be one of the way that the exosomes induce macrophages into M2 polarization (Fig. 5E).

4. Discussion

Tissue engineering scaffolds with guide tissue regeneration and control the tissue structure in damaged parts have played a vital role in tissue engineering. Biomaterials are the basis of scaffold forming and designing. Foreign body reaction caused by immune system is the main factor limiting the use of scaffolds [40–43]. Although many methods have been developed to minimize the immune interactions with scaffolds including the use of inert materials and bionic design, such as PCL inert scaffolds and biomimetic scaffolds including progenitor cells, growth factors, and extracellular matrix (ECM) structural component,

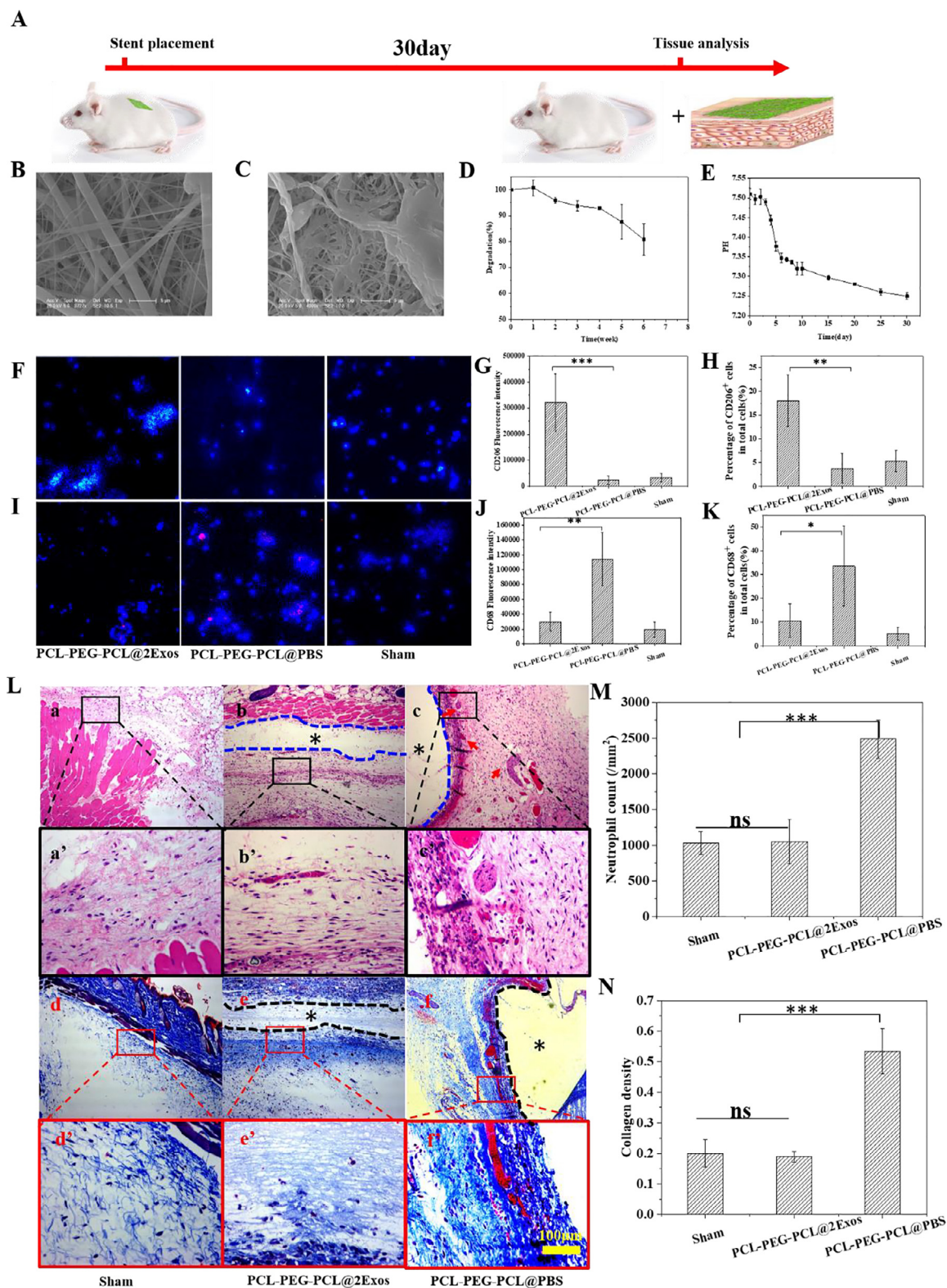


Fig. 4. Bioactive engineered scaffolds inhibit foreign body reaction *in vivo*. (A) Flow chart of implantation experiment. (B), (C) SEM images of PCL-PEG-PCL scaffolds and PCL-PEG-PCL scaffolds soaked in PBS for 30 days, respectively. (D) The weight change of PCL-PEG-PCL scaffolds soaked in PBS. (E) The pH change of the solution soaked PCL-PEG-PCL scaffolds. (F), (I) The confocal laser image of the tissue around the scaffold (green:CD206; red:CD86; blue: Cell nuclear), respectively. (G) and (J) are the quantification of the fluorescence intensity of CD206 and CD86, respectively. (H) and (K) are the percentage of CD206⁺ cells and CD86⁺ cells in total cells. (L)The H&E staining (a,a',b,b',c,c') and the Masson staining (d,d',e,e',f,f') of the tissue around the scaffold. The . is where the scaffold is placed. (M) Neutrophil count of tissue in sham, PCL-PEG-PCL@2Exo and PCL-PEG-PCL@PBS group. (N) Collagen density of tissue in sham, PCL-PEG-PCL@2Exo and PCL-PEG-PCL@PBS group. The data are shown as the means ± S.D. from three independent experiments (with three replicates each); *p < 0.05, **p < 0.01, ***p < 0.001 indicates significant differences between the indicated columns.

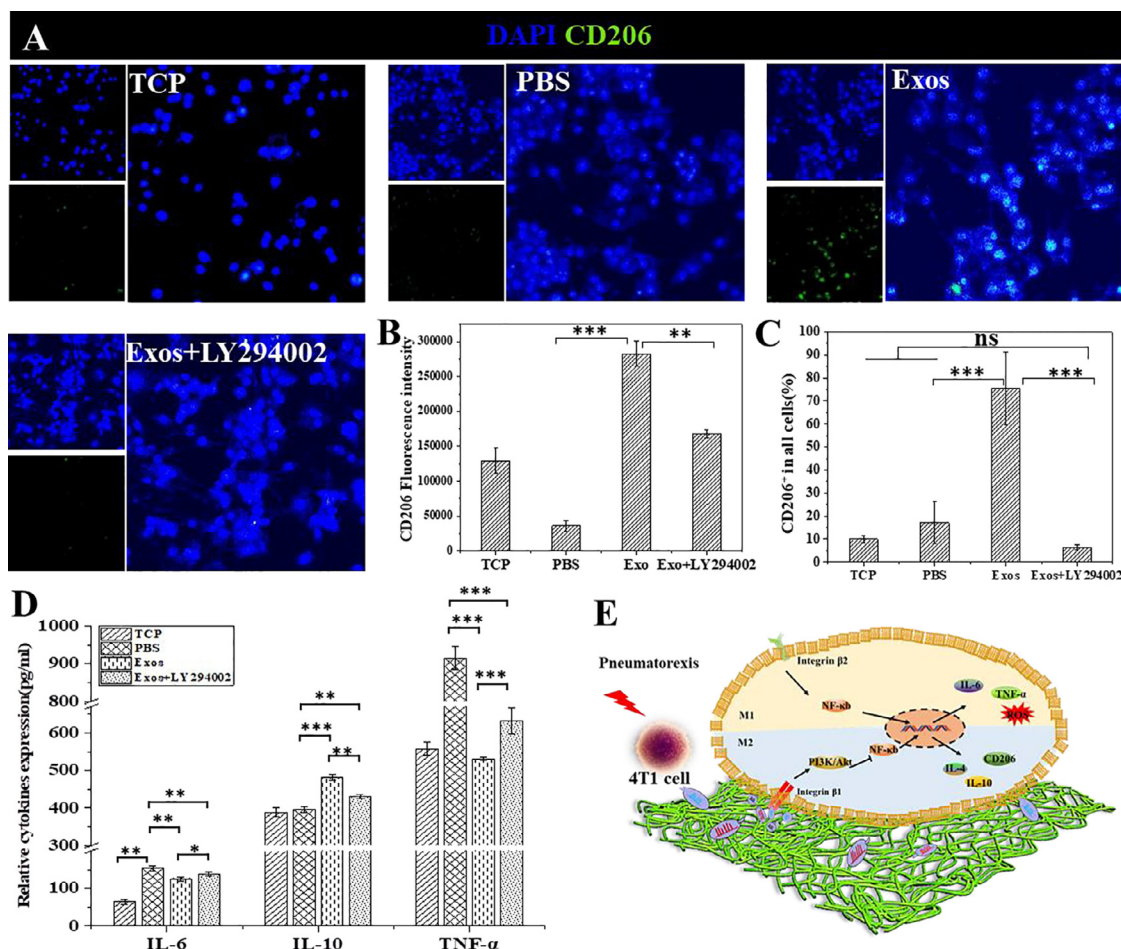


Fig. 5. Exosomes promote macrophage M2 polarization via Akt/PI3K. (A) Confocal laser images of macrophages after different treatments with PBS, Exos and LY294002. (B) Quantization of CD206 fluorescence intensity in confocal. (C) The proportion of CD206 positive cells in total cells. (D) The concentration of IL-6, IL-10, TNF- α in cell supernatant of different groups. (E) Exosomes promote the polarization of macrophages by activating the PI3K/Akt signaling pathway. The data are shown as the means \pm S.D. from three independent experiments (with three replicates each); * p <0.05, ** p <0.01 and *** p <0.001 indicates significant differences between the indicated columns.

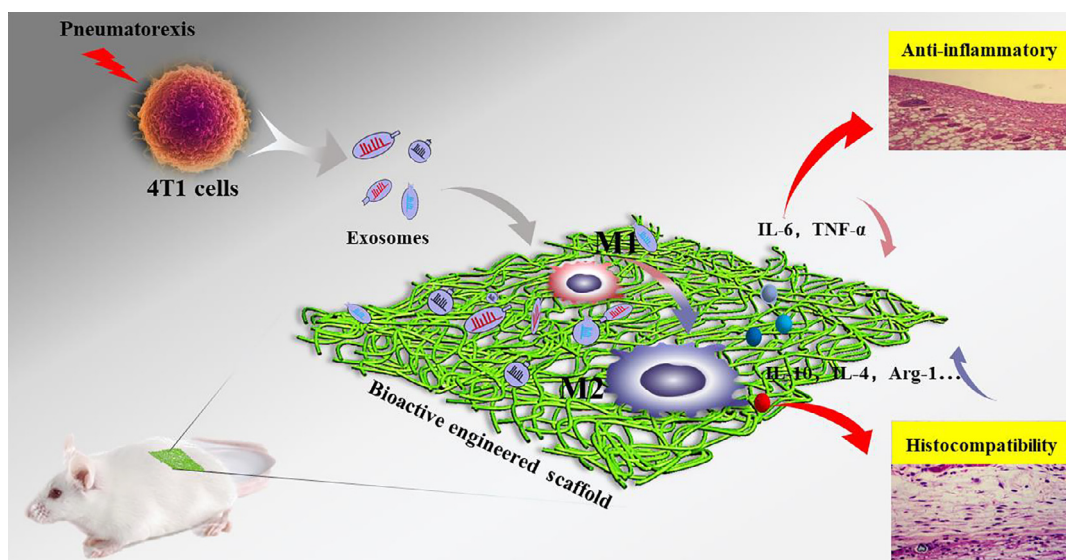
the successful inhibition of foreign body reactions is still lacking [44–51]. Further research showed that macrophages quickly migrate to the surface of the material and polarize pro-inflammatory M1 phenotype when materials are implanted into body. The prolonged M1 presence causes a severe FBR, resulting in chronic inflammation and failure of implantation. Inspired by that tumor cells induce macrophages from M1 polarization to M2 polarization through exosomes, we use cancer cells-derived exosomes as loader on implanted biomaterials to inhibit the FBR. In brief, mouse breast cancer cell-derived exosomes are loaded on PCL-PEG-PCL fiber scaffolds to fabricate bioactive engineered scaffolds. The function of exosome was verified with mouse and mouse cells. The exosomes are demonstrated to induce macrophages around the implanted biomaterials to M2 polarization, and minimize the unnecessary immune reaction of the body (Scheme 1).

Characteristics of the protein and morphology demonstrate that we successfully obtain exosomes of 4T1 cell [52], and the size is about 50nm. The 4T1 cell-derived exosomes show good anti-inflammatory activity by promote the macrophage into M2 polarization (Fig. 1). Biocompatibility and safety are essential for biomaterials in clinical [53,54]. Due to the particularity of exosome source, the carcinogenicity and effect to promote cancerous are researched in Figs. S1 and S2. Although studies have shown that cancer cell exosomes contain more oncogenes and can induce gene recombination in cell level [55,56], we preliminarily demonstrate the safety of exosomes at the *in vivo* level. Exosomes neither accelerate the metastasis of the primary tumor nor cause cancer

in the organism. Of course, because the complexity of cancer pathogenesis and development, the safety of exosomes needs further research.

The biodegradability and bioinertia of polycaprolactone make it more and more widely concerned in tissue engineering [57]. The excellent mechanical properties of PCL fiber scaffolds mean that PCL fiber scaffolds can be used as the matrix of many scaffolds (Fig. S5) [58,59]. Next, we show the even attachment of exosomes on PCL-PEG-PCL fiber scaffold as well as the exosomes' sustained release profile from scaffold *in vitro*. Almost all exosomes are released within the first 3 days. At the cellular level, bioactive fiber scaffold can regulate macrophages into M2 polarization and the efficiency of polarization is related to quantity of exosome loaded (Fig. 3). The optimal load is about 1.5 μ g to 2 μ g. The air-pouch model of inflammation is used to verify the anti-inflammatory ability of PCL-PEG-PCL@Exo scaffolds *in vivo* according to the method of Rafique et al. [36]. The short-term anti-inflammatory effect of scaffolds *in vivo* is very obvious, which gives us confidence to study its long-term application.

PCL-PEG-PCL fiber scaffold degrades by 15% within one month *in vitro* and lowers PH of microenvironment (Fig. 4 B–E), since minor changes in extracellular PH can considerably influence the synthesis of matrix macromolecules [60], the gradual degradation of scaffolds and PH reduction cause inflammation inevitably which is also an important factor of FBR. But many researches have shown that the degradation rate of polycaprolactone is slow. In fact, it is widely accepted that hydrolytic degradation of PCL can proceed via surface or bulk degradation



Scheme 1. Schematic diagram of bioactive engineered scaffold with cancer cell-derived exosomes to promote M2 polarization.

pathways, the diffusion–reaction phenomenon determines the means by which this pathway proceed [57]. The excellent hydrophilicity of the PCL-PEG-PCL fiber scaffold allows water to enter the fiber and accelerates the hydrolysis.

Neutrophils first arrive at the inflammatory site and produce an inflammatory response, after which macrophages migrate to the implant surface and polarize into M1 phenotype to promote the development of inflammation, and neutrophils further aggregate. Macrophages and neutrophils coordinate with each other to achieve immune function [61–63]. And M2 macrophages can mediate inflammation resolution by releasing anti-inflammatory factors, such as IL-4 and IL-10 etc [10]. The formation of multinucleated giant cells and fibrotic tissue around the scaffold are the most important characteristics of FBR [64,65]. No neutrophil aggregation, multinucleated giant cells appeared and low collagen density near the bioactive engineered scaffolds after the scaffold was implanted subcutaneously for 1 month means exosomes loaded on scaffold reduce inflammation and FBR (Fig. 4E).

Our work further expands the understanding of how exosomes exert macrophage immunomodulation. Considering the complexity of the function of cancer cell exosomes, we used the exclusion method to explore the mechanism of exosomes mediating macrophage M2. When the Akt/PI3K pathway is inhibited, the release of anti-inflammatory factors and polarization of macrophages were significantly reduced (Fig. 5). So we could preliminarily judge that the Akt/PI3K pathway is one of the pathways of exosomes mediated M2 polarization. The action mechanism is shown in Fig. 5E. But due to the complexity of tumor exosome inclusion and the diversity of functions, there must be many other mechanisms of exosomes [66]. Here, we just explore the mechanism of exosome preliminarily, and the specific mechanism may need further research.

5. Conclusions

In summary, inspired by the special capability of tumor exosomes in macrophages M2 polarization, we designed PCL-PEG-PCL scaffolds loaded with cancer cell-derived exosomes to construct bioactive engineered scaffolds for macrophages polarization. We demonstrated tumor exosomes exhibited no carcinogenicity and metastasis for normal mouse within 6 months. The exosomes were loaded on the PCL-PEG-PCL scaffolds with physical adsorption and the exosomes released gradually from scaffold after implantation; the exosomes reacted actively with the macrophages around the scaffolds to facilitate macrophages polariza-

tion in M2 phenotype through PI3K/Akt signaling pathway. As a result, cancer cell-derived exosomes show the potential for constructing bioactive engineered scaffolds in inhibiting the excessive inflammation and facilitating tissue formation.

Declaration of Competing Interest

The authors declare that they have no known competing financial interests or personal relationships that could have appeared to influence the work reported in this paper.

Acknowledgements

This work was supported by the financial support of the National Natural Science Foundation of China (52061135202, 51573186), National Key Research and Development Program of China (2018YFE0121400), and Open Research Fund of State Key Laboratory of Polymer Physics and Chemistry in CIAC, CAS (2020-19).

Supplementary materials

Supplementary material associated with this article can be found, in the online version, at doi:10.1016/j.bbiosy.2022.100055.

References

- [1] Herraiz S, Romeu M, Buigues A, Martinez S, Diaz-Garcia C, Gomez-Segui I, Martinez J, Pellicer N, Pellicer A. Autologous stem cell ovarian transplantation to increase reproductive potential in patients who are poor responders. *Fertil Steril* 2018;110(3):496–505. doi:10.1016/j.fertnstert.2018.04.025.
- [2] Zhang F, King MW. Biodegradable polymers as the pivotal player in the design of tissue engineering scaffolds. *Adv Healthc Mater* 2020;9(13):e1901358. doi:10.1002/adhm.201901358.
- [3] Osaki T, Sivathanu V, Kamm RD. Crosstalk between developing vasculature and optogenetically engineered skeletal muscle improves muscle contraction and angiogenesis. *Biomaterials* 2018;156:65–76. doi:10.1016/j.biomaterials.2017.11.041.
- [4] Li X, Cho B, Martin R, Seu M, Zhang C, Zhou Z, Choi JS, Jiang X, Chen L, Walia G, Yan J, Callanan M, Liu H, Colbert K, Morrissette-McAlmon J, Grayson W, Reddy S, Sacks JM, Mao HQ. Nanofiber-hydrogel composite-mediated angiogenesis for soft tissue reconstruction. *Sci Transl Med* 2019;11(490). doi:10.1126/scitranslmed.aau6210.
- [5] Diegelmann RF, Evans MC. Wound healing: an overview of acute, fibrotic and delayed healing. *Front Biosci* 2004;1(1):283–9. <https://www.researchgate.net/publication/329375441>.
- [6] Bygd HC, Ma L, Bratlie KM. Physicochemical properties of liposomal modifiers that shift macrophage phenotype. *Mater Sci Eng C Mater Biol Appl* 2017;79:237–44. doi:10.1016/j.msec.2017.05.032.

- [7] Nakkala JR, Yao Y, Zhai Z, Duan Y, Zhang D, Mao Z, Lu L, Gao C. Dimethyl itaconate-loaded nanofibers rewrite macrophage polarization, reduce inflammation, and enhance repair of myocardial infarction. *Small* 2021;17(17):e2006992. doi:10.1002/sml.202006992.
- [8] Sica A, Mantovani A. Macrophage plasticity and polarization: *in vivo* veritas. *J Clin Invest* 2012;122(3):787–95. doi:10.1172/JCI59643.
- [9] Wynn TA, Barron L. Macrophages: master regulators of inflammation and fibrosis. *Semin Liver Dis* 2010;30(3):245–57. doi:10.1055/s-0030-1255354.
- [10] Vishwakarma A, Bhise NS, Evangelista MB, Rouwkema J, Dokmeci MR, Ghaemmaghami AM, Vrana NE, Khademhosseini A. Engineering immunomodulatory biomaterials to tune the inflammatory response. *Trends Biotechnol* 2016;34(6):470–82. doi:10.1016/j.tibtech.2016.03.009.
- [11] Chung L, Maestas DR, Housseau F, Elisseeff JH. Key players in the immune response to biomaterial scaffolds for regenerative medicine. *Adv Drug Deliv Rev* 2017;114:184–92. doi:10.1016/j.addr.2017.07.006.
- [12] Julier Z, Park AJ, Briquet PS, Martino MM. Promoting tissue regeneration by modulating the immune system. *Acta Biomater* 2017;53:13–28. doi:10.1016/j.actbio.2017.01.056.
- [13] Dziki JL, Badylak SF. Immunomodulatory biomaterials. *Curr Opin Biomed Eng* 2018;6:51–7. doi:10.1016/j.cobme.2018.02.005.
- [14] Sridharan R, Cameron AR, Kelly DJ, Kearney CJ, O'Brien FJ. Biomaterial based modulation of macrophage polarization: a review and suggested design principles. *Mater Today* 2015;18(6):313–25. doi:10.1016/j.mattod.2015.01.019.
- [15] Kahler C, Melo SA, Protopopov A, Tang J, Seth S, Koch M, Zhang J, Weitz J, Chin L, Futreal A, Kalluri R. Identification of double-stranded genomic DNA spanning all chromosomes with mutated KRAS and p53 DNA in the serum exosomes of patients with pancreatic cancer. *J Biol Chem* 2014;289(7):3869–75. doi:10.1074/jbc.C113.532267.
- [16] Valadi H, Ekstrom K, Bossios A, Sjostrand M, Lee JJ, Lotvall JO. Exosome-mediated transfer of mRNAs and microRNAs is a novel mechanism of genetic exchange between cells. *Nat Cell Biol* 2007;9(6):654–9. doi:10.1038/ncb1596.
- [17] Balaj L, Lessard R, Dai L, Cho YJ, Pomeroy SL, Breakfield XO, Skog J. Tumour microvesicles contain retrotransposon elements and amplified oncogene sequences. *Nat Commun* 2011;2:180. doi:10.1038/ncomms1180.
- [18] Wubbolts R, Leckie RS, Veenhuizen PTM, Schwarzmann G, Möbius W, Hoerschemeyer J, Slot J-W, Geuze HJ, Stoorvogel W. Proteomic and biochemical analyses of human B cell-derived exosomes. *J Biol Chem* 2003;278(13):10963–72. doi:10.1074/jbc.M207550200.
- [19] Wolfers J, Lozier A, Raposo G, Regnault A, Thery C, Masurier C, Flament C, Poupieux S, Faure F, Tursz T, Angevin E, Amigorena S, Zitvogel L. Tumor-derived exosomes are a source of shared tumor rejection antigens for CTL cross-priming. *Nat Med* 2001;7(3):297–303. doi:10.1038/85438.
- [20] Lancaster GI, Febbraio MA. Exosome-dependent trafficking of HSP70: a novel secretory pathway for cellular stress proteins. *J Biol Chem* 2005;280(24):23349–55. doi:10.1074/jbc.M502017200.
- [21] Wang X, Luo G, Zhang K, Cao J, Huang C, Jiang T, Liu B, Su L, Qiu Z. Hypoxic tumor-derived exosomal miR-301a mediates M2 macrophage polarization via PTEN/PI3Kgamma to promote pancreatic cancer metastasis. *Cancer Res* 2018;78(16):4586–98. doi:10.1158/0008-5472.CAN-17-3841.
- [22] Goswami KK, Ghosh T, Ghosh S, Sarkar M, Bose A, Baral R. Tumor promoting role of anti-tumor macrophages in tumor microenvironment. *Cell Immunol* 2017;316:1–10. doi:10.1016/j.cellimm.2017.04.005.
- [23] Grafahrend D, Heffels KH, Beer MV, Gasteier P, Möller M, Boehm G, Dalton PD, Groll J. Degradable polyester scaffolds with controlled surface chemistry combining minimal protein adsorption with specific bioactivation. *Nat Mater* 2011;10(1):67–73. doi:10.1038/nmat2904.
- [24] Xiang Z, Chen R, Ma Z, Shi Q, Ataullakhanov FI, Pantelev M, Yin J. A dynamic remodeling bio-mimic extracellular matrix to reduce thrombotic and inflammatory complications of vascular implants. *Biomater Sci* 2020;8(21):6025–36. doi:10.1039/d0bm01316a.
- [25] Okano T, Nishiyama S, Shinohara I, Akaike T, Sakurai Y, Kataoka K, Tsuruta T. Effect of hydrophilic and hydrophobic microdomains on mode of interaction between block polymer and blood. *J Biomed Mater Res* 1981;15(3):393–402. doi:10.1002/jbm.820150310.
- [26] Plebanek MP, Angeloni NL, Vinokour E, Li J, Henkin A, Martinez-Marin D, Filleul S, Bhowmick R, Henkin J, Miller SD, Ifergan I, Lee Y, Osman I, Thaxton CS, Volpert OV. Pre-metastatic cancer exosomes induce immune surveillance by patrolling monocytes at the metastatic niche. *Nat Commun* 2017;8(1):1319. doi:10.1038/s41467-017-01433-3.
- [27] Hoshino A, Costa-Silva B, Shen TL, Rodrigues G, Hashimoto A, Tesic Mark M, Molina H, Kohsaka S, Di Giannatale A, Ceder S, Singh S, Williams C, Soplop N, Uryu K, Pharmed L, King T, Bojmar L, Davies AE, Ararso Y, Zhang T, Zhang H, Hernandez J, Weiss JM, Dumont-Cole VD, Kramer K, Wexler LH, Narendran A, Schwartz GK, Healey JH, Sandstrom P, Labori KJ, Kure EH, Grandgenett PM, Hollingsworth MA, de Sousa M, Kaur S, Jain M, Mallya K, Batra SK, Jarnagin WR, Brady MS, Fodstad O, Muller V, Pantel K, Minn AJ, Bissell MJ, Garcia BA, Kang Y, Rajasekhar VK, Ghajar CM, Matei I, Peinado H, Bromberg J, Lyden D. Tumour exosome integrins determine organotropic metastasis. *Nature* 2015;527(7578):329–35. doi:10.1038/nature15756.
- [28] Zhang H, Deng T, Liu R, Bai M, Zhou L, Wang X, Li S, Wang X, Yang H, Li J, Ning T, Huang D, Li H, Zhang L, Ying G, Ba Y. Exosome-delivered EGFR regulates liver microenvironment to promote gastric cancer liver metastasis. *Nat Commun* 2017;8:15016. doi:10.1038/ncomms15016.
- [29] de Souza Garcia CM, de Araújo MR, Lopes MTP, Ferreira MAND, Cassali GD. Morphological and immunophenotypical characterization of murine mammary carcinoma 4T1. *Braz J Vet Pathol* 2014;7(3):158–65. https://bjvp.org.br/wp-content/uploads/2015/07/DOWNLOAD-FULL-ARTICLE-4-20881_2014_11_29_44_20.pdf.
- [30] Nag S, Resnick A. Stabilization of hypoxia inducible factor by cobalt chloride can alter renal epithelial transport. *Physiol Rep* 2017;5(24):e13531. doi:10.14814/phy2.13531.
- [31] Hsieh CH, Tai SK, Yang MH. Snail-overexpressing cancer cells promote M2-like polarization of tumor-associated macrophages by delivering MiR-21 abundant exosomes. *Neoplasia* 2018;20(8):775–88. doi:10.1016/j.neo.2018.06.004.
- [32] Pan X, Lu Y, Lan R, Liu Z, Qin Z, Wang H, Liu Z. Mitosis detection techniques in H&E stained breast cancer pathological images: a comprehensive review. *Comp Electr Eng* 2021;91:107038. doi:10.1016/j.compeleceng.2021.107038.
- [33] Yang S, Tang Z, Hu C, Zhang D, Shen N, Yu H, Chen X. Selectively potentiating hypoxia levels by combretastatin A4 nanomedicine: toward highly enhanced hypoxia-activated prodrug tirapazamine therapy for metastatic tumors. *Adv Mater* 2019;31(11):e1805955. doi:10.1002/adma.201805955.
- [34] Wang Y, Li L, Zhao W, Dou Y, An H, Tao H, Xu X, Jia Y, Lu S, Zhang J, Hu H. Targeted therapy of atherosclerosis by a broad-spectrum reactive oxygen species scavenging nanoparticle with intrinsic anti-inflammatory activity. *ACS Nano* 2018;12(9):8943–60. doi:10.1021/acsnano.8b02037.
- [35] Huleihel L, Hussey GS, Naranjo JD, Zhang L, Dziki JL, Turner NJ, Stolz DB, Badylak SF. Matrix-bound nanovesicles within ECM bioscaffolds. *Sci Adv* 2016;2(6):e1600502. doi:10.1126/sciadv.1600502.
- [36] Rafique M, Wei T, Sun Q, Midgley AC, Huang Z, Wang T, Shafiq M, Zhi D, Si J, Yan H, Kong D, Wang K. The effect of hypoxia-mimicking responses on improving the regeneration of artificial vascular grafts. *Biomaterials* 2021;271:120746. doi:10.1016/j.biomaterials.2021.120746.
- [37] Wu G, Zhang J, Zhao Q, Zhuang W, Ding J, Zhang C, Gao H, Pang DW, Pu K, Xie HY. Molecularly engineered macrophage-derived exosomes with inflammation tropism and intrinsic heme biosynthesis for atherosclerosis treatment. *Angew Chem* 2020;59:4068–74. <https://www.ncbi.nlm.nih.gov/pubmed/31854064>.
- [38] Vasconcelos DP, Costa M, Amaral IF, Barbosa MA, Aguiar AP, Barbosa JN. Modulation of the inflammatory response to chitosan through M2 macrophage polarization using pro-resolution mediators. *Biomaterials* 2015;37:116–23. doi:10.1016/j.biomaterials.2014.10.035.
- [39] Lv L, Xie Y, Li K, Hu T, Lu X, Cao Y, Zheng X. Unveiling the mechanism of surface hydrophilicity-modulated macrophage polarization. *Adv Healthc Mater* 2018;7(19):e1800675. doi:10.1002/adhm.201800675.
- [40] Langer R. Biomaterials in drug delivery and tissue engineering: one laboratory's experience. *Acc Chem Res* 2000;33(2):94–101. doi:10.1021/ar9800993.
- [41] Lam J, Clark EC, Fong EL, Lee EJ, Lu S, Tabata Y, Mikos AG. Evaluation of cell-laden polyelectrolyte hydrogels incorporating poly(L-Lysine) for applications in cartilage tissue engineering. *Biomaterials* 2016;83:332–46. doi:10.1016/j.biomaterials.2016.01.020.
- [42] Mitragotri S, Burke PA, Langer R. Overcoming the challenges in administering biopharmaceuticals: formulation and delivery strategies. *Nat Rev Drug Discov* 2014;13(9):655–72. doi:10.1038/nrd4363.
- [43] Morais JM, Papadimitrakopoulos F, Burgess DJ. Biomaterials/tissue interactions: possible solutions to overcome foreign body response. *AAPS J* 2010;12(2):188–96. doi:10.1208/s12248-010-9175-3.
- [44] Zhang G. Biomimicry in biomedical research. *Organogenesis* 2012;8(4):101–2. doi:10.4161/org.23395.
- [45] Fan D, De Rosa E, Murphy MB, Peng Y, Smid CA, Chiappini C, Liu X, Simmons P, Weiner BK, Ferrari M, Tasciotti E. Mesoporous silicon-PLGA composite microspheres for the double controlled release of biomolecules for orthopedic tissue engineering. *Adv Funct Mater* 2012;22(2):282–93. doi:10.1002/adfm.201100403.
- [46] Minardi S, Taraballi F, Pandolfi L, Tasciotti E. Patterning biomaterials for the spatiotemporal delivery of bioactive molecules. *Front Bioeng Biotechnol* 2016;4:45. doi:10.3389/fbioe.2016.00045.
- [47] Klarmann GJ, Gaston J, Ho VB. A review of strategies for development of tissue engineered meniscal implants. *Biomater Biosyst* 2021;4:100026. doi:10.1016/j.bbiosy.2021.100026.
- [48] Minardi S, Corradetti B, Taraballi F, Sandri M, Martinez JO, Powell ST, Tampieri A, Weiner BK, Tasciotti E. Biomimetic concealing of PLGA microspheres in a 3D scaffold to prevent macrophage uptake. *Small* 2016;12(11):1479–88. doi:10.1002/sml.201503484.
- [49] Murphy MB, Blashki D, Buchanan RM, Fan D, De Rosa E, Shah RN, Stupp SI, Weiner BK, Simmons PJ, Ferrari M, Tasciotti E. Multi-composite bioactive osteogenic sponges featuring mesenchymal stem cells, platelet-rich plasma, nanoporous silicon enclosures, and peptide amphiphiles for rapid bone regeneration. *J Funct Biomater* 2011;2(2):39–66. doi:10.3390/jfb2020039.
- [50] Pandolfi L, Furman NT, Wang X, Lupo C, Martinez JO, Mohamed M, Taraballi F, Tasciotti E. A nanofibrous electrospun patch to maintain human mesenchymal cell stemness. *J Mater Sci Mater Med* 2017;28(3):44. doi:10.1007/s10856-017-5856-0.
- [51] Taraballi F, Bauza G, McCulloch P, Harris J, Tasciotti E. Concise review: biomimetic functionalization of biomaterials to stimulate the endogenous healing process of cartilage and bone tissue. *Stem Cells Transl Med* 2017;6(12):2186–96. doi:10.1002/sctm.17-0181.
- [52] Qi C, Liu X, Zhi D, Tai Y, Liu Y, Sun Q, Wang K, Wang S, Midgley AC, Kong D. Erratum to: Exosome-mimicking nanovesicles derived from efficacy-potented stem cell membrane and secretome for regeneration of injured tissue. *Nano Res* 2022. doi:10.1002/sctm.17-0181.
- [53] Yu W, Maynard E, Chiaradia V, Arno MC, Dove AP. Aliphatic polycarbonates from cyclic carbonate monomers and their application as biomaterials. *Chem Rev* 2021;121(18):10865–907. doi:10.1021/acs.chemrev.0c00883.
- [54] Li J, Chen Q, Zhang Q, Fan T, Gong L, Ye W, Fan Z, Cao L. Improving mechanical properties and biocompatibilities by highly oriented long chain branch-

- ing poly(lactic acid) with bionic surface structures. *ACS Appl Mater Interfaces* 2020;12(12):14365–75. doi:10.1021/acsami.9b20264.
- [55] Antonyak MA, Li B, Boroughs LK, Johnson JL, Druso JE, Bryant KL, Holowka DA, Cerione RA. Cancer cell-derived microvesicles induce transformation by transferring tissue transglutaminase and fibronectin to recipient cells. *Proc Natl Acad Sci USA* 2011;108(12):4852–7. doi:10.1073/pnas.1017667108.
- [56] Abd Elmageed ZY, Yang Y, Thomas R, Ranjan M, Mondal D, Moroz K, Fang Z, Rezk BM, Moparty K, Sikka SC, Sartor O, Abdel-Mageed AB. Neoplastic reprogramming of patient-derived adipose stem cells by prostate cancer cell-associated exosomes. *Stem Cells* 2014;32(4):983–97. doi:10.1002/stem.1619.
- [57] Woodruff MA, Hutmacher DW. The return of a forgotten polymer-polycaprolactone in the 21st century. *Prog Polym Sci* 2010;35(10):1217–56. doi:10.1016/j.progpolymsci.2010.04.002.
- [58] Shuai C, Liu G, Yang Y, Qi F, Peng S, Yang W, He C, Wang G, Qian G. A strawberry-like Ag-decorated barium titanate enhances piezoelectric and antibacterial activities of polymer scaffold. *Nano Energy* 2020;74:104825. doi:10.1016/j.nanoen.2020.104825.
- [59] Shuai C, Xu Y, Feng P, Wang G, Xiong S, Peng S. Antibacterial polymer scaffold based on mesoporous bioactive glass loaded with *in situ* grown silver. *Chem Eng J* 2019;374:304–15. doi:10.1016/j.cej.2019.03.273.
- [60] Wu MH, Urban JP, Cui ZF, Cui Z, Xu X. Effect of extracellular pH on matrix synthesis by chondrocytes in 3D agarose gel. *Biotechnol Prog* 2007;23(2):430–4. doi:10.1021/bp060024v.
- [61] Butterfield TA, Best TM, Merrick MA. The dual roles of neutrophils and macrophages in inflammation: a critical balance between tissue damage and repair. *J Athl Train* 2006;41(4):457–65. <https://www.ncbi.nlm.nih.gov/pmc/articles/PMC1748424>.
- [62] Silva MT, Correia-Neves M. Neutrophils and macrophages: the main partners of phagocyte cell systems. *Front Immunol* 2012;3:174. doi:10.3389/fimmu.2012.00174.
- [63] Back M, Yurdagul A, Tabas I, Oorni K, Kovanen PT. Inflammation and its resolution in atherosclerosis: mediators and therapeutic opportunities. *Nat Rev Cardiol* 2019;16(7):389–406. doi:10.1038/s41569-019-0169-2.
- [64] Luttkhuizen DT, Dankers PY, Harmsen MC, van Luyn MJ. Material dependent differences in inflammatory gene expression by giant cells during the foreign body reaction. *J Biomed Mater Res A* 2007;83(3):879–86. doi:10.1002/jbm.a.31420.
- [65] Sheikh Z, Brooks PJ, Barzilay O, Fine N, Glogauer M. Macrophages, foreign body giant cells and their response to implantable biomaterials. *Materials* 2015;8(9):5671–701 (Basel). doi:10.3390/ma8095269.
- [66] Kalluri R. The biology and function of exosomes in cancer. *J Clin Investig* 2016;126(4):1208–15. doi:10.1172/JCI81135.